materials

MDPI

Article

Covalent Organic Framework (C_6N_6) as a Drug Delivery Platform for Fluorouracil to Treat Cancerous Cells: A DFT Study

Mohammed A. Alkhalifah [1,*], Muhammad Yar [2], Imene Bayach [1], Nadeem S. Sheikh [3] and Khurshid Ayub [2,*]

[1] Department of Chemistry, College of Science, King Faisal University, Al-Ahsa 31982, Saudi Arabia
[2] Department of Chemistry, COMSATS University Islamabad, Abbottabad Campus, Abbottabad 22060, KPK, Pakistan
[3] Chemical Sciences, Faculty of Science, Universiti Brunei Darussalam, Jalan Tungku Link, Gadong BE1410, Brunei
* Correspondence: malkalifah@kfu.edu.sa (M.A.A.); khurshid@cuiatd.edu.pk (K.A.)

Abstract: Continuous studies are being carried out to explore new methods and carrier surfaces for target drug delivery. Herein, we report the covalent triazine framework C_6N_6 as a drug delivery carrier for fluorouracil (FU) and nitrosourea (NU) anti-cancer drugs. FU and NU are physiosorbed on C_6N_6 with adsorption energies of −28.14 kcal/mol and −27.54 kcal/mol, respectively. The outcomes of the non-covalent index (NCI) and quantum theory of atoms in molecules (QTAIM) analyses reveal that the FU@C_6N_6 and NU@C_6N_6 complexes were stabilized through van der Waals interactions. Natural bond order (NBO) and electron density difference (EDD) analyses show an appreciable charge transfer from the drug and carrier. The FU@C_6N_6 complex had a higher charge transfer (−0.16 e^-) compared to the NU@C_6N_6 complex (−0.02 e^-). Frontier molecular orbital (FMO) analysis reveals that the adsorption of FU on C_6N_6 caused a more pronounced decrease in the HOMO-LUMO gap (E_{H-L}) compared to that of NU. The results of the FMO analysis are consistent with the NBO and EDD analyses. The drug release mechanism was studied through dipole moments and pH effects. The highest decrease in adsorption energy was observed for the FU@C_6N_6 complex in an acidic medium, which indicates that FU can easily be off-loaded from the carrier (C_6N_6) to a target site because the cancerous cells have a low pH compared to a normal cell. Thus, it may be concluded that C_6N_6 possesses the therapeutic potential to act as a nanocarrier for FU to treat cancer. Furthermore, the current study will also provide motivation to the scientific community to explore new surfaces for drug delivery applications.

Keywords: drug delivery; cancer; covalent triazine framework C_6N_6; density functional theory

Citation: Alkhalifah, M.A.; Yar, M.; Bayach, I.; Sheikh, N.S.; Ayub, K. Covalent Organic Framework (C_6N_6) as a Drug Delivery Platform for Fluorouracil to Treat Cancerous Cells: A DFT Study. *Materials* **2022**, *15*, 7425. https://doi.org/10.3390/ma15217425

Academic Editor: Ziyad S. Haidar

Received: 28 September 2022
Accepted: 17 October 2022
Published: 22 October 2022

1. Introduction

Cancer is a leading cause of death worldwide and poses a serious threat to public health. To deal with this daunting disease, several therapies, such as chemotherapy, hormone therapy, and radiotherapy [1] are in use. However, these therapies have several associated side effects. Some of the common side effects are breast and throat swelling, anemia, blurred vision, pain, nausea, hair loss, fatigue, skin and mood changes, stomach bloating, and vaginal bleeding [2]. Furthermore, the application of diverse antineoplastic drugs has been explored to evaluate their efficacy to destroy cancerous cells [3,4]. Undoubtedly, some of the extensively used anti-cancerous drugs in the pharmaceutical sector include nitrosourea (NU), 5-fluorouracil (FU), and their derivatives [5–9]. Despite their remarkable therapeutic properties, normal cells are prone to harmful effects if these drugs are used at high concentrations. This has been reported for the conventional chemotherapeutic methods, which suffer from a lack of specificity and lead to the destruction of normal cells along with melanotic cells [10,11]. Considering this, it is vital to efficiently control the plasma concentration of antineoplastic drugs via an effective and targeted drug delivery system (DDS). The dosage of anti-cancerous drugs can be adjusted according to the given

circumstances, including the severity of the disease and the patient's tolerance level in targeted DDS [12–14].

Owing to the significance of DDSs in medicinal chemistry, the development of innovative and highly effective DDSs with improved therapeutic profiles is inevitable. Arguably, the application of DDSs has gained enormous attention as one of the most promising and efficient methods reported for the treatment of cancer and which abates the severely harmful side effects of the conventional approaches to cancer treatment [15]. One of the key features of DDSs involves the administration of a controlled dosage of drugs to target the tumor cells without noticeable degradation of the drug molecules [16–19]. Among the various approaches that are used for DDS, chronopharmacology is one of them. With chronopharmacology, the drug is delivered to a patient through a staggered profile system [20]. Subsequently, the protonation of the drug molecule influenced by the acidic environment of the cancerous tissues weakens the binding interaction of the drug with the carrier and results in an effective off-loading of the drug molecule from the carrier to the cancerous tissues [21]. As expected, this therapeutic protocol is thwarted by some serious challenges, including poor absorption and compromised biocompatibility of the drug molecules on the carrier surface [22].

Gratifyingly, recent progress in the field of nanotechnology has revolutionized almost every aspect of research and has substantially contributed to the diagnosis and treatment of several deadly diseases. In addition, controlled drug delivery has been carried out both experimentally and numerically. In a reported study, the controlled drug release of gliclazide from a polymeric matrix system was studied [23]. Numerous reports have highlighted the selective attack of nanoparticles on cancerous cells without producing toxic effects on normal cells [24–26]. Due to the extensive research executed in this area, the nanoparticle-based drug delivery system (NDDS) has emerged as a highly efficient, well-controlled, and target-oriented protocol [27]. Moreover, the NDDS reveals an enormous potential in cancer treatment by providing a reasonable solution to the poor absorption problem [9] and has demonstrated several advantages, including a prolonged half-life, better bio-distribution, controlled and preserved drug release, a better circulation time of the drug, and versatility in the modes of administration [28–31]. Extracellular vesicles, which naturally carry endogenous bioactive nucleic acids, are also capable of transferring small interfering RNAs to the target cancer cells [32]. In addition, a large number of near-infrared light-sensitive drug delivery systems have been successfully devised, which have showcased promising results for the treatment of cancer [16].

The ubiquitous presence of computational investigation to better understand and elaborate the research findings is beyond any doubt, and the field is attracting serious attention from the scientific community day by day. In-depth theoretical studies have played a pivotal role in the development of DDSs as well, and their contribution is on the rise. For example, Samanta et al. explored the application of a fullerene (C_{60}) surface for temozolomide and carmustine and reported that the release of these chemotherapeutic drugs to biological systems is considerably facilitated by the enhanced polarity of C_{60} when attached to these anti-cancer drugs [33]. Mechanistically, several factors contribute to a facile release of drugs that are primarily dependent on the nature of the drug carrier, type of affinity (either chemical or physical), and the morphological features of the drugs under investigation. Some of the commonly reported mechanisms associated with the release of drug molecules from nanocarriers highlight the role of diffusion, solvent, chemical reaction, and stimuli-controlled processes [34–36]. Over the past decade, different types of NDDS have been reported that demonstrate the use of silver, gold [37], iron oxide [38], dendrimers [39], polymeric micelles [40,41], liposomes [42,43], quantum dots [44], and carbon nanotubes [45,46] as nanocarriers for the drug molecules. At the present time, ultrathin two-dimensional materials, such as graphene and its derivatives (graphene oxide, reduced graphene), transition metal dichalcogenides, hexagonal boron nitride, Mxenes (monolayers of Si, Ge, and Sn), and phosphorenes, are extensively used NDDSs due to their remarkable mechanical, electrical, and optical properties, in addition to their enhanced

surface area [47–49]. In general, 2D materials exhibit great potential for drug delivery due to a high surface area for drug loading [50–53]. There have been several reports in the literature that shed light on the successful application of 2D materials in DDSs. Yang et al., for instance, theoretically investigated the use of phosphorene and hexagonal boron nitride nanosheets as DDSs for fluorouracil and mercaptopurine, respectively [32]. More recently, Mohammed et al. demonstrated the potential of pristine graphene and metal-doped graphene nanosheets as DDSs for various potent anti-cancer drugs, including 6-mercaptopurine cyclophosphamide and fluorouracil [33]. Another DFT investigation highlighted the use of fluorinated graphene oxide as an efficient carrier for doxorubicin and camptothecin, similar to a study that reported on the use of silver- and gold-coated iron nanoparticles (for the delivery of mercaptopurine and cisplatin) and silicone oxide nanoparticles (for the delivery of gemcitabine) [28,54].

As detailed above, the fundamental and challenging issues faced during the delivery of anti-cancer drugs with macrosystems are poor absorption and poor biocompatibility in specific regions due to the lack of the optimal adsorption of the drug molecule onto the surface of the drug carrier. Nanostructures that have been studied experimentally for drug delivery systems are primarily metal alloys and quantum dots, which have low biocompatibility due to their hydrophobic nature [55]. Carbon nitrides were recently reported to have a mix of hydrophobic and hydrophilic natures, with a high surface-to-volume ratio, which is helpful for finding their applications in drug delivery systems. Among these, carbon nitride, C_6N_6, is the one with the highest nitrogen contents and is expected to have quite good hydrophilicity. Therefore, we became interested in studying the application of C_6N_6 for drug delivery. Moreover, high nitrogen contents can provide good binding of the drug molecules to the C_6N_6 surface. Owing to our continuous interest in the development of an efficient drug delivery system for anti-cancer drug molecules [55,56], herein, we report our investigation of a two-dimensional covalent triazine framework (C_6N_6) as a drug delivery platform for NU and FU. The reports in the literature have revealed that C_6N_6 has not yet been investigated as a DDS for the FU and NU anti-cancerous drugs. Our proposed system can effectively interact with the targeted drugs because of its unique characteristics related to an electron-rich cavity and high surface area [57]. The current study theoretically examined the nature of the interactions between anti-cancerous drugs FU and NU with C_6N_6, which are commonly used for cancer treatments. DFT simulations have been applied to study the mechanism of drug delivery and to provide a detailed investigation of the electronic properties of this class of materials, as well as a better understanding of the nature of the interactions between the studied drug molecules and the triazine framework.

2. Computational Methodology

All the simulations in the current study were carried out by employing Gaussian 09 software. The geometries of the C_6N_6 and Drug@C_6N_6 complexes were computed at a ωb97XD/6-31++G (d, p) level of theory. ωb97XD is range-separated functional that is considered best for non-covalent interactions [56]. In ωb97XD, the ω is a function of range-separation, which efficiently reduces self-interaction error [57]. Moreover, ωb97XD includes Grimme's D2 dispersion model to effectively capture van der Waals interactions [57]. The electronic properties, such as frontier molecular orbitals (FMO), the natural bond order (NBO), and the electron density difference (EDD) for all the complexes were performed at the same level of theory [58–61]. Drug molecules are adsorbed on C_6N_6 by different orientations to find the most stable geometry of each complex. Frequency analysis was carried out to confirm the true minimum nature of each optimized complex on the potential energy surface. The adsorption energies of Drug@C_6N_6 were calculated as:

$$\Delta E = [E_{(complex)} - (E_{C6N6} + E_{Drug})]$$

where $E_{complex}$ is the energy of the Drug@C_6N_6 complex, E_{C6N6} is the energy of C_6N_6, and E_{Drug} is the drug molecule. The nature of the interactions between the drugs and C_6N_6

was explored by non-covalent interaction (NCI) analysis. NCI analysis mainly comprises a reduced density gradient (RDG), the product of the electron density (ρ), and the sign of λ_2. The RDG is a product of the density and its derivative, which is represented as [62].

$$s = \frac{1}{2(3\pi^2)^{\frac{1}{3}}} \frac{\nabla\rho}{\rho^{4/3}}$$

In non-covalent interactions, the electron density (ρ) is small. Thus, a small change in density gives a noticeable change in the RDG scale. The strength and nature of non-covalent interactions are explored through product (λ_2) ρ. So, the nature of the NCI depends on the sign and value of λ_2. If the product of (λ_2) ρ is large and negative, electrostatic interactions appear in the form of blue spikes in low RDG regions. If (λ_2) ρ is negative and small (below −0.02 a.u.), NCIs are projected in the form of green spikes, which indicate the presence of van der Waals interactions. The large and positive values of (λ_2) ρ show repulsive interactions and are projected in the form of red spikes [63–65].

Quantum theory of atoms in molecules (QTAIM) analysis provides detailed information about inter- and intra-molecular interactions. Through QTAIM analysis, various types of topological terms, such as bond critical points (BCPs), ring critical points (RCPs), cage critical points (CCPs), and nuclear critical points (NCPs) can be explored. Bond critical points are usually applied to describe the nature of NCIs. Various parameters, such as the electron density (ρ), the Laplacian of the electron density ($\nabla^2\rho$), the potential energy density (V), the local kinetic energy density (G), and the electronic energy density (H) are used to explain the BCPs [66]. The interactions are covalent in nature when ρ is greater than 0.1 a.u. and ($\nabla^2\rho$) is large and negative. On the other hand, $\rho < 0.1$ a.u. and a positive ($\nabla^2\rho$) value reveals close shell interactions [67,68]. Multiwfn 3.7 software was employed for the NCI, QTAIM, and EDD analyses [69]. The dipole moment and pH effects were also studied for the drug delivery of FU and NU at target sites by the C_6N_6 carrier.

3. Results and Discussion

3.1. Geometry Optimization and Interaction Energy

Initially, we optimized the cluster model of C_6N_6 through DFT simulations (see Figure 1). Bond distances of 1.53 Å and 1.33 Å were observed for the C-C and C-N bonds of the C_6N_6 monolayer, respectively (Figure 1). The observed bond distances are in good agreement with the already reported experimental and theoretical studies [70]. Each monolayer unit of C_6N_6 consists of covalently bonded s-triazine rings. The s-triazine rings contain nitrogen atoms, which makes the cavity of C_6N_6 highly electron rich. The diameter of the cavity in C_6N_6 is 5.46 Å (between two nitrogen atoms) [71]. The highly electron-rich nitrogenated cavity of C_6N_6 makes it a potential candidate for drug loading and delivery at target sites. The geometries of the selected anti-cancerous drugs (fluorouracil and nitrosourea; see Figure 1) were also optimized at the same level of theory (ωb97XD/6–31++G (d,p)). FU is an antimetabolite drug, which works by inhibiting essential biosynthetic processes or by being incorporated into macromolecules such as DNA and RNA. FU performs both functions. In the initial step, 5-FU exerts its anticancer effects through the inhibition of thymidylate synthase (TS) and the incorporation of its metabolites into DNA (see Figure 1) [72]. On other hand, nitrosourea is an alkylating agent with a long history in cancer treatment. Its mechanism of action is represented by the alkylation of DNA strands, which results in DNA damage and cellular death [73]. So, in both drugs, DNA is ultimately the common receptor.

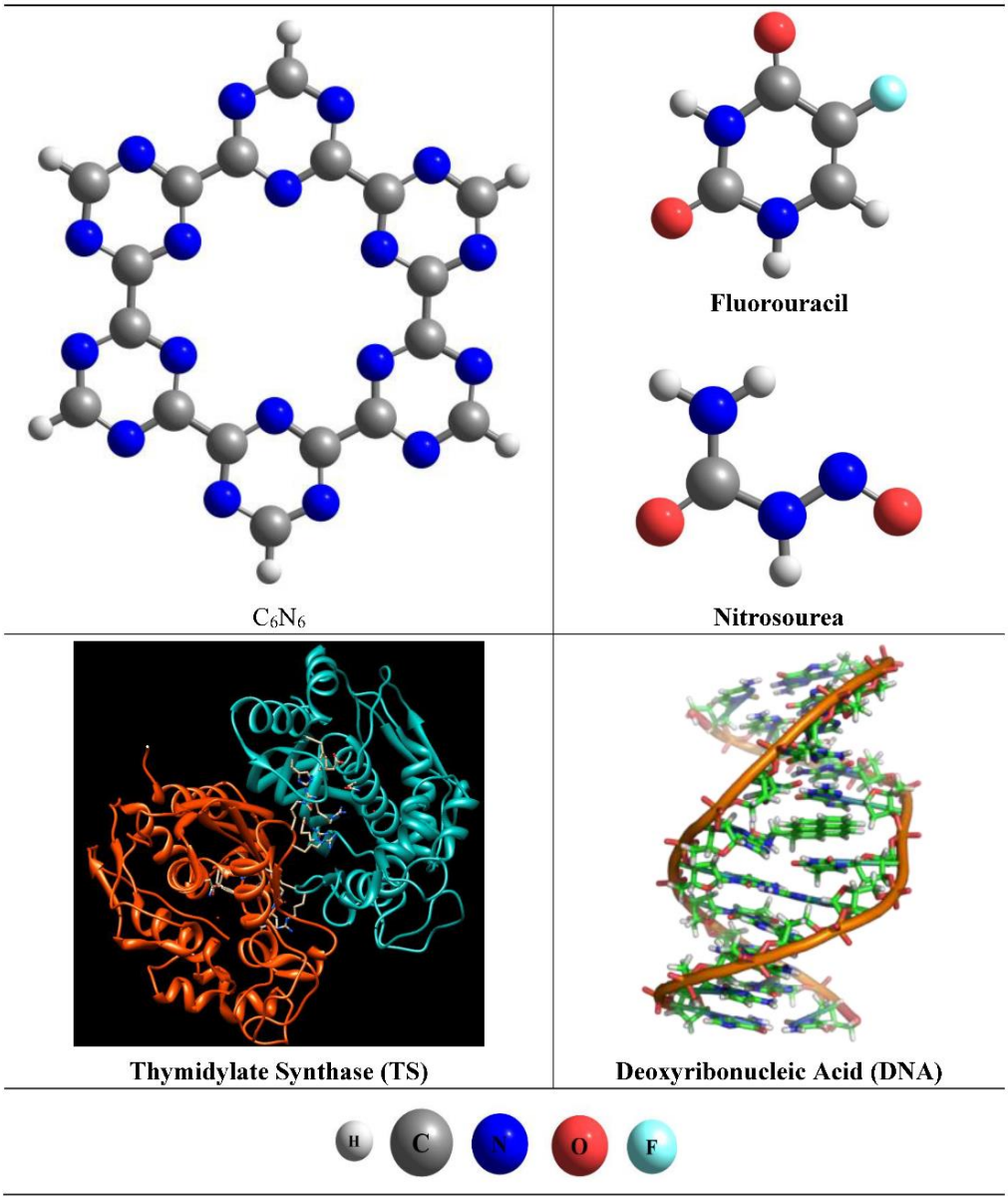

Figure 1. Optimized geometries of cluster model of C_6N_6, fluorouracil, and uracil at ωb97XD/6-31++G (d,p) level of theory. General representation of anti-cancerous drug receptors thymidylate synthase (TS) and deoxyribonucleic acid.

Fluorouracil and nitrosourea were relaxed over C_6N_6 in different orientations to obtain the most stable Drug@C_6N_6 complexes for effective drug delivery at a specified target. The resultant most stable geometries of the Drug@C_6N_6 complexes are reported in Figure 2, while the less stable complexes of Drug@C_6N_6 are shown in the Supplementary Materials (Figure S1). Furthermore, the energies of the most stable Drug@C_6N_6 complexes are provided in Table 1, whereas all others are given in the Supplementary Materials (Table S1).

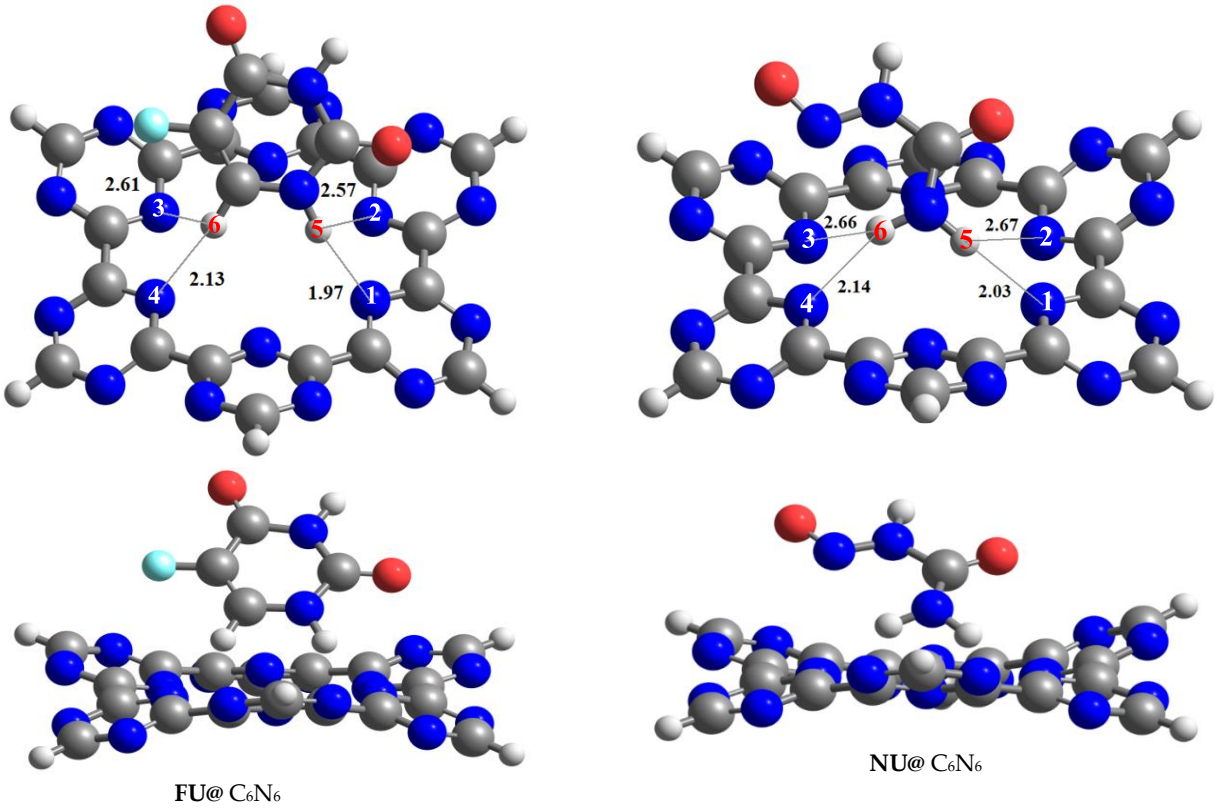

Figure 2. Top and tiled views of optimized geometries of most stable complexes of FU@C_6N_6 and NU@C_6N_6 at ωb97XD/6–31++G (d,p) level of theory.

Table 1. Adsorption energies (kcal/mol) and geometric parameters of the most stable geometries of FU@C_6N_6 and NU@C_6N_6 complexes at ωb97XD/6-31++G (d,p) level of theory.

Drug@ C_6N_6	Drugs–C_6N_6	Adsorption Distance (Å)	Adsorption Energy (kcal/mol)
FU@C_6N_6	H5–N1	1.97	−28.14
	H5–N2	2.57	
	H6–N3	2.13	
	H6–N4	2.61	
NU@C_6N_6	H5–N1	2.03	−26.57
	H5–N2	2.67	
	H6–N3	2.66	
	H6–N4	2.14	

The most stable complexes of FU@C_6N_6 and NU@C_6N_6 resulted in adsorption energies of −28.14 kcal/mol and −26.57 kcal/mol, respectively. The stable geometries of both drug complexes were obtained as a result of the interaction of the H-atoms of the drugs with the N-atoms of the C_6N_6. This happened due to the electron-rich cavity of the C_6N_6 surface and the electrophilic nature of the H-atoms of the drug molecules. The adsorption energy values of the FU@C_6N_6 and NU@C_6N_6 complexes reveal that both drugs had strong binding with the C_6N_6 surface.

The adsorption energy of the most stable complex of the FU@C_6N_6 complex (−28.14 kcal/mol) was comparatively higher than that of the NU@C_6N_6 complex (−26.57 kcal/mol). The stable complex of the FU@C_6N_6 was obtained due to the shorter interaction distances of 1.97 Å (H5–N1) and 2.13 Å (H6–N3) between the H-atoms of the fluorouracil and the N-atoms of the C_6N_6. The rest of the H–N interaction distances noticed

in the FU@C_6N_6 were 2.57 Å (H5–N2) and 2.61 Å (H6–N4). The interaction distances between the H-atoms of the NU and the N-atoms of the C_6N_6 were 2.03 Å (H5–N1) and 2.14 Å (H6–N4), which are slightly higher than those of the FU@C_6N_6 complex. The adsorption energies and interaction distances show the stability of the FU@C_6N_6 and NU@C_6N_6 complexes through physisorption, which is best for the C_6N_6 surface to act as a drug delivery platform.

3.2. Non-Covalent Interaction (NCI) Analysis

To differentiate between the electrostatic, van der Waals, and repulsive interactions between the drugs and C_6N_6, NCI analysis was performed. The results of the NCI analysis were displayed in 3D topological forms and 2D RDG plots. The topologies and RDG plots of the FU@C_6N_6 and NU@C_6N_6 complexes are presented in Figure 3. In the 3D topologies, the green and light brown patches show the stability of the FU@C_6N_6 and NU@C_6N_6 complexes by van der Waals interactions (see Figure 3). The red cylinder projections in the triazine rings of C_6N_6 indicate the ring's steric strain. The thickness and area of green patches between the drugs and C_6N_6 are not the same, which reveals that the drug molecules (FU and NU) interacted with C_6N_6 via different energies.

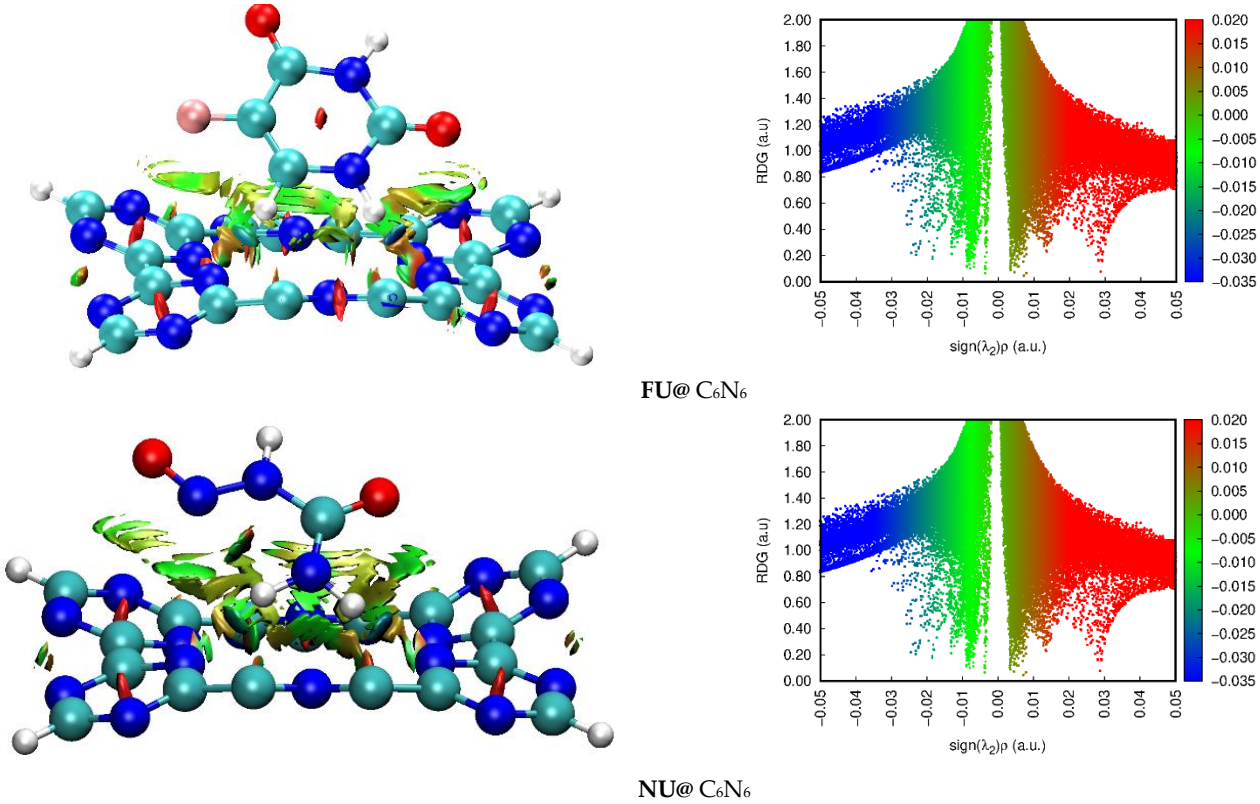

Figure 3. Three-dimensional isosurfaces and 2D RDG plots of FU@C_6N_6 and NU@C_6N_6 complexes at iso value of 0.002 a.u.

In the case of the FU@C_6N_6, the green patches in the 3D plot are not specified between any two atoms of the drug and C_6N_6, but rather distributed among many atoms. The 3D topology of the FU@C_6N_6 reveals that the thick and wide green patches between the H-atoms of the FU and the N-atoms of the C_6N_6 caused stronger interactions and higher stability of the FU@C_6N_6 compared to the NU@C_6N_6 complex. Similarly, the mixture of the bluish-green spikes in the 2D RDG plot of the FU@C_6N_6 increases up to −0.02 a.u., whereas, in the case of the NU@C_6N_6, the green spikes are in the range of −0.02 to −0.01 a.u., which further justifies the higher stability of the FU@C_6N_6 complex than that of the NU@C_6N_6 complex. Therefore, the NCI analysis shows that both complexes were stabilized by van der Waals interactions. These interactions may facilitate the off-loading of the drug to the target site.

3.3. Quantum Theory of Atoms in Molecule (QTAIM) Analysis

Through QTAIM analysis, we can capture all the non-covalent interactions that are elusive to other methods. The strength of NCI mainly depends upon the sign and value of the electron density (ρ) and the Laplacian of the electron density ($\nabla^2\rho$). In addition, the potential energy density (V), kinetic energy density, and their sum (which is described by the total energy density (H)) give valuable information about the BCPs. V/G is the ratio of the potential energy density (V) to the kinetic energy density (G). A V/G less than 1 indicates NCIs. In addition, an individual bond interaction energy of >-3.5 kcal/mol (negatively strong) shows shared shell interactions [74–77].

The topologies obtained through the QTAIM analysis are presented in Figure 4, while the values of the BCP parameters are given in Table 2. In the QTAIM analysis of FU and NU, the numbers of BCPs observed were seven (07) and eight (08), respectively. These numbers actually represent the possible number of non-covalent interactions between the FU (and NU) with the C_6N_6. The values of the BCP parameters presented in Table 2 show that the stability of the FU@C_6N_6 complex happened not only through van der Waal interactions but also through the observed participation of electrostatic interactions. In the NU@C_6N_6 complex, the number of BCPs observed was eight, but the ρ and ($\nabla^2\rho$) values were comparatively lower than those of the FU@C_6N_6 complex. Similarly, the rest of the BCP parameter values of the NU@C_6N_6 were also low compared to those of the FU@C_6N_6. Thus, the high stability of the FU complex was a result of the high values of ρ and ($\nabla^2\rho$). These BCP parameters reveal that FU could easily be adsorbed on the carrier surface compared to NU. The results obtained through the QTAIM analysis are in good agreement with those of the interaction energies and NCI analysis.

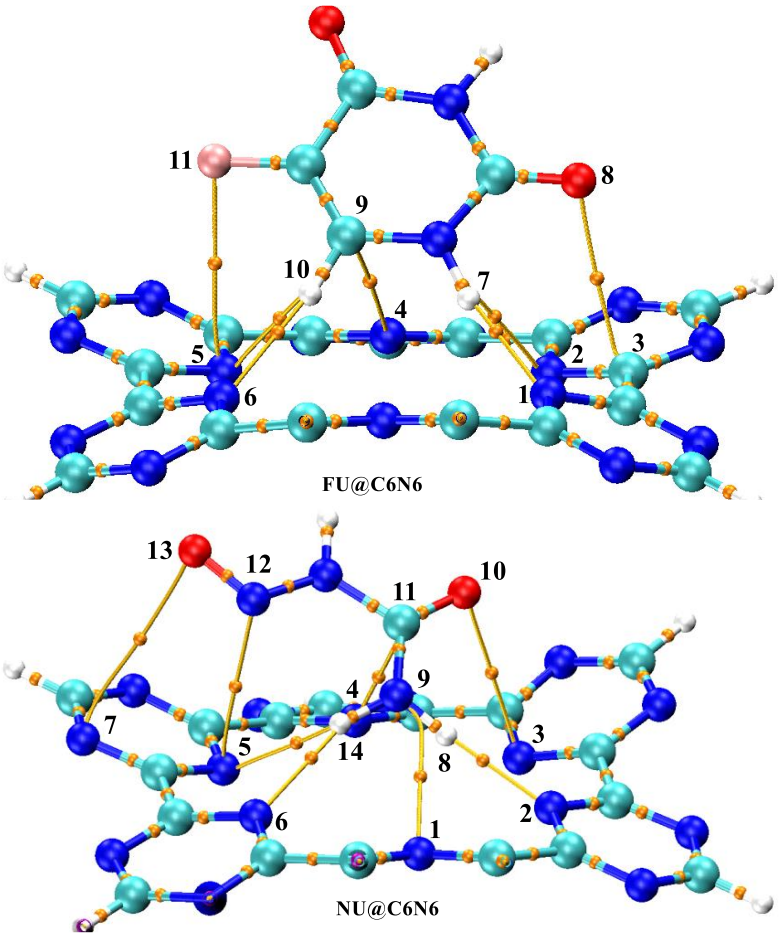

Figure 4. QTAIM analysis of FU@C_6N_6 and NU@C_6N_6.

Table 2. Topological analysis of FU@C_6N_6 and NU@C_6N_6 obtained through QTAIM analysis.

Drugs@C_6N_6	Drug–C_6N_6	ρ	$\nabla^2\rho$	G (r)	V (r)	H (r)	V(r)/G(r)	Eint (kcal/mole)
FU@C_6N_6	H7-N1	0.027	0.072	0.011	−0.010	0.0010	0.91	−3.17
	H7-N2	0.010	0.035	0.007	−0.006	0.0013	0.82	−1.91
	O8-C3	0.010	0.034	0.008	−0.007	0.0009	0.88	−2.09
	C4-N4	0.007	0.021	0.004	−0.004	0.0008	0.83	−1.15
	F11-N5	0.005	0.022	0.005	−0.004	0.0009	0.80	−1.15
	H10-N5	0.009	0.034	0.007	−0.005	0.0016	0.77	−1.63
	H10-N6	0.021	0.057	0.014	−0.014	0.0002	0.99	−4.34
NU@C_6N_6	H9-N1	0.008	0.032	0.007	−0.005	0.0014	0.79	−1.65
	H8-N2	0.024	0.067	0.017	−0.012	0.0041	0.75	−3.91
	O10-N3	0.009	0.030	0.007	−0.006	0.0006	0.90	−1.91
	C11-N4	0.008	0.030	0.006	−0.005	0.0013	0.80	−1.57
	N12-N5	0.009	0.027	0.006	−0.005	0.0007	0.88	−1.66
	O13-N7	0.004	0.015	0.003	−0.002	0.0006	0.79	−0.75
	H14-N5	0.007	0.026	0.006	−0.004	0.0011	0.80	−1.38
	H14-N6	0.008	0.032	0.007	−0.005	0.0014	0.79	−1.65

3.4. Natural Bond Orbital (NBO) and Electron Density Differences (EDD) Analyses

NBO and EDD analyses give valuable information about charge transfer in interacting systems. The magnitude of the charge transfer between the drug and C_6N_6 was explored through NBO analysis. The EDD was calculated by subtracting the sum of the drug and C_6N_6 charges from the charges of the Drug@C_6N_6 complex. The isosurfaces resulting from the EDD analysis consisted of two colors: green and yellow. The green isosurfaces indicate the accumulation of electron density, whereas the yellow surfaces show the depletion of electron density. So, the existence of both types of isosurfaces reveals the exchange of charges between the drug and C_6N_6. The isosurfaces executed through the EDD analysis are given in Figure 5. However, the values of charges obtained by the NBO analysis are shown in Table 3.

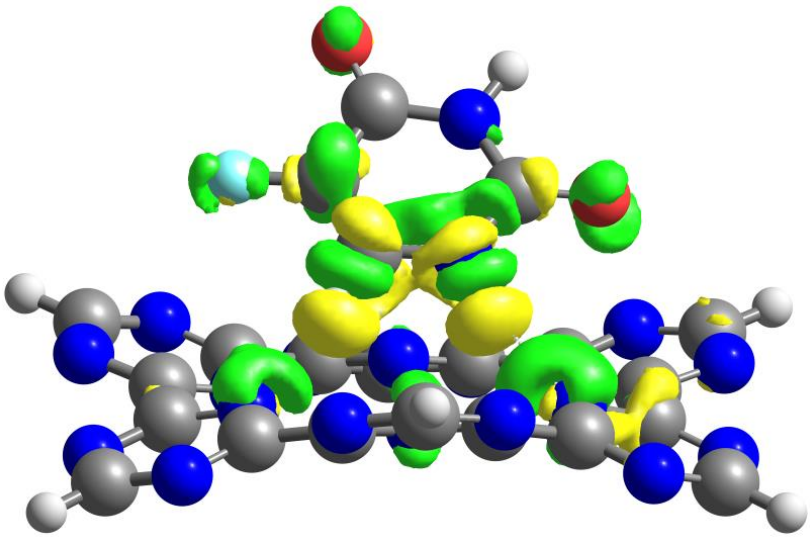

FU@ C_6N_6

Figure 5. *Cont.*

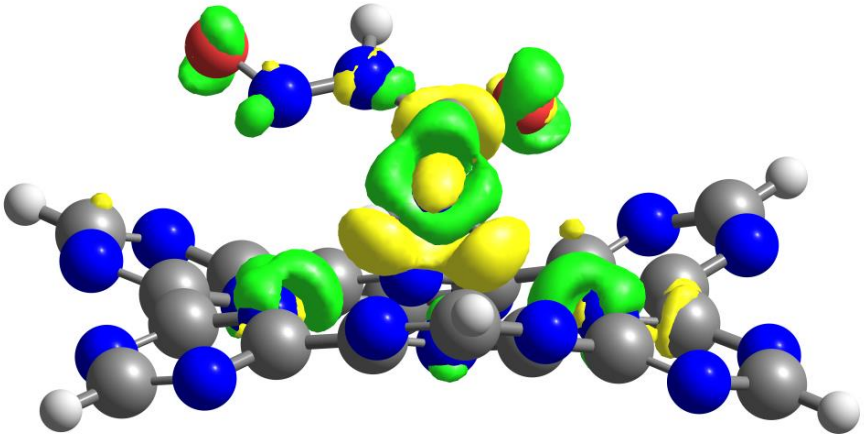

NU@ C_6N_6

Figure 5. Isosurface plots of FU@C_6N_6 and NU@C_6N_6 complexes obtained by EDD analysis. Isovalue = 0.0014 a. u.

Table 3. Values of HOMO, LUMO, E_{H-L} gap, and NBO for FU@C_6N_6 and NU@C_6N_6 complexes.

Drug@C_6N_6	HOMO	LUMO	E_{H-L} gap (eV)	NBO (e^-)
C_6N_6	−9.63	−1.79	7.84	
FU@C_6N_6	−8.63	−1.92	6.71	−0.16
NU@C_6N_6	−9.32	−1.78	7.54	−0.02

The NBO charge values of the FU and NU in the FU@C_6N_6 and NU@C_6N_6 complexes were −0.16 e^- and −0.02 e^-, respectively. The signs of the NBO charges reflect that the charge was transferred from the C_6N_6 to the drug molecules. This happened due to the electron-rich cavity of the covalent triazine framework C_6N_6. A higher charge transfer value was noticed in the case of the FU@C_6N_6, which indicates stronger interactions between the FU and C_6N_6 compared to the complex of NU@C_6N_6. The higher NBO value on the FU@C_6N_6 complex was due to the presence of highly electronegative F and O atoms in the FU. In addition to this, the FU interacted with the C_6N_6 through shorter interaction distances compared to those of the NU atoms. The NBO values were verified by EDD analysis.

In the case of the FU@C_6N_6 and NU@C_6N_6 complexes, green isosurfaces mainly appeared on the N-atoms of the C_6N_6, showing an accumulation of electron density, whereas yellow isosurfaces appeared on the H-atoms, showing depletion of the electron density. The yellow isosurfaces on the H-atoms were due to their bonding with the O-atoms of the C_6N_6 and interactions with the N-atoms of the C_6N_6. This shows that charges were transferred from the triazine ring of the C_6N_6 to the FU and NU atoms. However, the drug atoms consist of both types of isosurfaces, which verifies the presence of electrophilic and nucleophilic ends on the drug. The NBO and EDD analyses indicate that the highest charge transfer was in the case of FU (−0.16 e^-), which is in good agreement with the NCI, QTAIM, and interaction energy analyses. The higher charge exchange between the FU and C_6N_6 indicates the balanced loading capacity of the C_6N_6 to FU compared to that of NU.

3.5. Frontier Molecular Orbital (FMO) Analysis

FMO analysis was carried out to analyze the changes in the electronic properties of the C_6N_6 before and after complexations with the drug molecules. The energies of the highest occupied molecular orbital (HOMO), the lowest unoccupied molecular orbital (LUMO), and the HOMO-LUMO gaps (E_{H-L}) of pristine C_6N_6 and Drug@C_6N_6 are given in Table 3.

The HOMO and LUMO energies of the C_6N_6 were −9.63 eV and −1.79 eV, respectively. The E_{H-L} gap of the C_6N_6 was 7.84 eV. A change in the E_{H-L} gap was noticed after the adsorption of drugs on the C_6N_6. Figure 6 depicts the orbital densities of the C_6N_6 and

Drug@C_6N_6 complexes. The $E_{H\text{-}L}$ gaps after the adsorption of FU and NU on the C_6N_6 were 6.71 eV (FU@C_6N_6) and 7.54 eV (NU@C_6N_6), respectively.

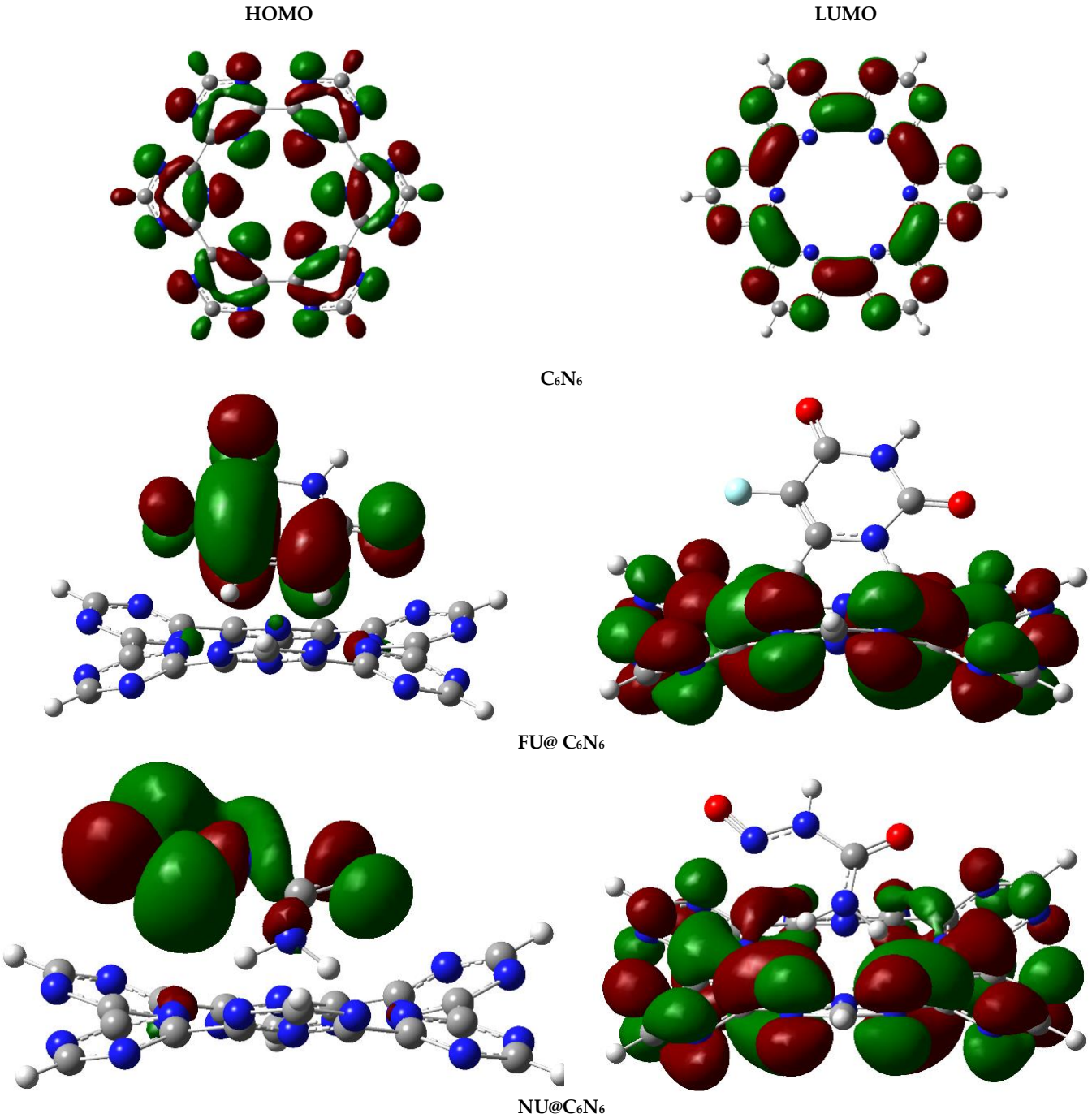

Figure 6. Orbital densities of FU@C_6N_6 and NU@C_6N_6 complexes obtained through FMO analysis (isovalue = 0.02 a.u.). Red isosurfaces show negative end of wavefunctions and green isosurfaces show positive wavefunctions.

Decreases in the $E_{H\text{-}L}$ gap were observed for the complexes of FU@C_6N_6 and NU@C_6N_6 compared to that of bare C_6N_6. The conductivity of the complexes depended on the $E_{H\text{-}L}$ gap. Complexes with a low $E_{H\text{-}L}$ gap showed better conductivity compared to those with a high $E_{H\text{-}L}$ gap. This reveals that the complex of FU@C_6N_6 had better conductance than that of the NU@C_6N_6 complex. The substantial decrease in the $E_{H\text{-}L}$ gap of the FU@CC_6N_6 happened due to a significant increase in the energy of the HOMO (from −9.63 to −8.63)

and a decrease in the energy of LUMO (from −1.79 eV to −1.92 eV), respectively. The $E_{H\text{-}L}$ gap for the NU@C_6N_6 complex was 7.54 eV, which was slightly lower than that of the bare C_6N_6 (7.84 eV). This happened due to a slight increase in the HOMO energy (−9.32 eV) while the LUMO energy remained almost unchanged (−1.78 eV).

The orbital isosurfaces for the complexes were also different compared to the pristine C_6N_6. The orbital densities of the FU@C_6N_6 and NU@C_6N_6 are presented in Figure 6. In the case of pristine C_6N_6, the HOMO densities were mainly distributed over the nitrogen atoms of the triazine rings, whereas the LUMO densities were on the carbon atoms. The orbital densities of the complexes show the charge transfer during the excitation from the HOMO to the LUMO. In the case of the FU@C_6N_6 complex, the HOMO density was majorly distributed over the FU, while a part of the HOMO density can also be seen in the C_6N_6. However, the LUMO was completely located on the C_6N_6, and the orbital density distribution pattern of the NU@C_6N_6 complex was slightly different from the FU@C_6N_6 complex. The maximum portion of the HOMO density was concentrated on the NU, while a small contribution was shown by the N-atoms of the C_6N_6, and the LUMO was fully distributed over the C_6N_6 surface. This shift of orbital densities from the FU (HOMO) to the C_6N_6 (LUMO) caused a significant decrease in the $E_{H\text{-}L}$ gap. Thus, it can be concluded that the adsorption of FU caused an increase in the electrical conductivity of the C_6N_6 surface. This significant increase in the conductivity of the FU@C_6N_6 complex makes C_6N_6 a promising carrier for drug delivery through electrical therapy. The drug delivery mechanism of dexamethasone (DEX) from polydopamine/polypyrrole composites has also been reported on a conductivity basis [78,79] The results of the FMO analysis are in good agreement with those of the interaction energy, NCI, QTAIM, NBO, and EDD analyses.

4. Dipole Moment (μ) Analysis

The change in the dipole moment also helps to explain the solubility of the drug and its release at the target site. The μ of C_6N_6 COF is zero prior to the loading of drugs. This may happen due to the symmetry in the structure and the cancelation of the individual dipoles. The adsorption of FU and NU over C_6N_6 changed the μ values to 5.77 D and 3.25 D, respectively in the resultant complexes. The symmetry of the C_6N_6 was disturbed by the adsorption of the FU and NU on C_6N_6. This adsorption created new dipoles on the electron-withdrawing and -donating parts of complexes, where the drug and carrier surfaces interact through specific distances. The increase in the **μ** of complexes is essential for their solubility in an aqueous medium, which also helps the mobility of drugs in a living system. The substantial increase in the μ of the FU@C_6N_6 complex reveals the high affinity of FU for biological systems compared to NU. This shows that C_6N_6 can effectively release FU on a target site compared to NU. The results of the **μ** are consistent with the FMO, NBO, interaction energy, and NCI analyses.

Comparison of Adsorption Energies of FU and NU with Different Surfaces

The adsorption energies of the FU@C_6N_6 (−28.14 kcal/mol) and NU@C_6N_6 (−27.54 kcal/mol) complexes were also compared with the already studied adsorption energies of FU and NU at different surfaces through different DFT tools. The reported adsorption energies of the drugs on different carriers are comparable to the values in the current study (FU@C_2N; −26.3 kcal/mol and NU@C_2N; −26.4 kcal/mol). In some cases, the adsorption energies were too high; FU@NaB40 fullerene and Ti-BNNT showed adsorption energies of −30.0 kcal/mol and −39.8 kcal/mole, respectively (see Table 4). These values of adsorption energies show that FU and NU can easily be off-loaded to the target site.

Table 4. Comparison of adsorption energies of FU@C_6N_6 and NU@C_6N_6 complexes with reported literature data on drug release.

DDS	DFT Functionals	Adsorption Energies (kcal/mol)
FU@C_2N	M06-2x	−26.3 [80]
NU@C_2N	M06-2x	−26.4 [80]
FU@B_{40} fullerene	PBE	−24.0 [81]
FU@NaB_{40} fullerene	PBE	−30.0 [81]
FU@Ti-BNNT	B3LY	−39.8 [82]
NU@BC_3	PW91	−20.3 [83]
NU@B_{40}	PBE0-D3	−25.1 [84]

5. Drug Release

The drug release from the carrier surface to the target cell is one of the most important steps. The surrounding environment of a malignant cell environment usually has a pH of less than 6 compared to normal blood cells (7.35–7.45) [46]. Thus, we explored the pH effect on the complexes of FU@C_6N_6 and FU@C_6N_6. We carried out DFT simulations of drugs (FU@C_6N_6 and NU@C_6N_6) loaded on C_6N_6 in an acidic environment. In an acidic medium, we protonated the interacted ends (N-atoms) of the C_6N_6 with H^+ and again relaxed the structure at the same level of theory. When comparing the FU@C_6N_6 and FU@C_6N_6 complexes in an acidic media, drastic decreases in the adsorption energies (from −28.14 to −1.15kcal/mole) and increases in the interaction distances (1.97 Å to 4.99 Å) were observed in the case of the FU@C_6N_6 complex. This indicates the easy off-loading of FU from the carrier (C_6N_6) to the target site compared to NU. In an acidic medium, a number of protons can also be attached to the other ends of the drug and surface. However, these protons may not affect the drug release at the target site.

6. Conclusions

To explore new drug delivery carriers, we used the covalent triazine framework C_6N_6 for FU and NU drugs through DFT simulations. Adsorption energies of −28.14 kcal/mol and −27.54 kcal/mol were observed in the most stable complexes of FU@C_6N_6 and NU@C_6N_6, respectively. The nature and strength of the non-covalent interactions were explored through NCI and QTAIM analyses. The outcomes of these analyses reveal that the stability of the FU@C_6N_6 and NU@C_6N_6 complexes was established through van der Waals interactions. The electronic properties of all the complexes were explored through NBO, EDD, and FMO analyses. Both the NBO and EDD analyses show an appreciable charge transfer between the drug and carrier. The FU@C_6N_6 complex had the highest charge transfer (−0.16 e^-), while the NU@C_6N_6 complex had the lowest charge exchange (−0.02 e^-). The $E_{H\text{-}L}$ gaps of the 6.71 eV and 7.54 eV were observed for the FU@C_6N_6 and NU@C_6N_6 complexes, which were comparatively lower than that of the bare C_6N_6 (7.84 eV). The adsorption of the FU on the C_6N_6 caused a potential decrease in the $E_{H\text{-}L}$ gap compared to that of the NU@C_6N_6. Thus, the loading of the FU on the C_6N_6 caused enhanced conductivity of the FU@C_6N_6 complex compared to that of the pristine C_6N_6. The results of the FMO analysis are consistent with those of the NBO, EDD, NCI, and QTAIM analyses. The drug release mechanisms were further studied through dipole moments and pH effects. Due to the low pH of malignant cells, simulations were performed in an acidic medium. The highest decrease in adsorption energy was observed for the FU@C_6N_6 complex in an acidic medium. These findings indicate that FU can easily be off-loaded from a carrier (C_6N_6) to a target site. Thus, it may be concluded that C_6N_6 is a better carrier of FU compared to NU for drug delivery.

Supplementary Materials: The following supporting information can be downloaded at: https://www.mdpi.com/article/10.3390/ma15217425/s1, Figure S1. Top and side views of least stable complexes of FU@C6N6 (a–c) and NU@C6N6 (d–f); Table S1. Adsorption energies of least stable complexes of drug@C6N6.

Author Contributions: Data curation, M.Y. and N.S.S.; Formal analysis, I.B., N.S.S.; Investigation, M.Y.; Methodology, I.B. and M.A.A.; Project administration, K.A. and M.A.A.; Resources, K.A; Software, K.A.; Validation, M.A.A.; Visualization, M.Y. and N.S.S.; Writing – original draft, M.A.A. and M.Y.; Writing – review & editing, K.A. All authors have read and agreed to the published version of the manuscript.

Funding: This work was supported by the Deanship of Scientific Research, Vice Presidency for Graduate Studies and Scientific Research, King Faisal University, Saudi Arabia [Grant No. 1234].

Data Availability Statement: All data are provided in the manuscript and in the supplementary material.

Acknowledgments: This work was supported by the Deanship of Scientific Research, Vice Presidency for Graduate Studies and Scientific Research, King Faisal University, Saudi Arabia [Grant No. 1234].

Conflicts of Interest: The authors declare no conflict of interest.

References

1. Sudhakar, A. History of Cancer, Ancient and Modern Treatment Methods. *J. Cancer Sci. Ther.* **2009**, *1*, 1–4. [CrossRef] [PubMed]
2. Aslam, M.S.; Naveed, S.; Ahmed, A.; Abbas, Z.; Gull, I.; Athar, M.A. Side Effects of Chemotherapy in Cancer Patients and Evaluation of Patients Opinion about Starvation Based Differential Chemotherapy. *J. Cancer Ther.* **2014**, *2014*, 48061. [CrossRef]
3. Molinelli, A.R.; Crews, K.R. Antineoplastic Drugs. In *Toxicology Cases for the Clinical and Forensic Laboratory*; Elsevier: Amsterdam, The Netherlands, 2020; pp. 141–150.
4. Wang, J.; Waxman, J. Chemotherapy for Prostate Cancer. *Urol. Oncol. Semin. Orig. Investig.* **2000**, *5*, 93–96. [CrossRef]
5. Laupacis, A. Efficacy of Adjuvant Fluorouracil and Folinic Acid in Colon Cancer. *Lancet* **1995**, *345*, 939–944. [CrossRef]
6. Gnewuch, C.T.; Sosnovsky, G. A Critical Appraisal of the Evolution of N -Nitrosoureas as Anticancer Drugs. *Chem. Rev.* **1997**, *97*, 829–1014. [CrossRef] [PubMed]
7. de Waard, J.W.D.; de Man, B.M.; Wobbes, T.; van der Linden, C.J.; Hendriks, T. Inhibition of Fibroblast Collagen Synthesis and Proliferation by Levamisole and 5-Fluorouracil. *Eur. J. Cancer* **1998**, *34*, 162–167. [CrossRef]
8. Pan, X.; Wang, C.; Wang, F.; Li, P.; Hu, Z.; Shan, Y.; Zhang, J. Development of 5-Fluorouracil Derivatives as Anticancer Agents. *Curr. Med. Chem.* **2011**, *18*, 4538–4556. [CrossRef]
9. Moertel, C.G. Gastrointestinal Cancer. Treatment with Fluorouracil-Nitrosourea Combinations. *JAMA J. Am. Med. Assoc.* **1976**, *235*, 2135–2136. [CrossRef]
10. Ross, J.S.; Schenkein, D.P.; Pietrusko, R.; Rolfe, M.; Linette, G.P.; Stec, J.; Stagliano, N.E.; Ginsburg, G.S.; Symmans, W.F.; Pusztai, L.; et al. Targeted Therapies for Cancer 2004. *Am. J. Clin. Pathol.* **2004**, *122*, 598–609. [CrossRef]
11. Morgillo, F.; Lee, H.-Y. Resistance to Epidermal Growth Factor Receptor-Targeted Therapy. *Drug Resist. Updates Rev. Comment. Antimicrob. Anticancer Chemother.* **2005**, *8*, 298–310. [CrossRef]
12. Huang, C.-Y.; Ju, D.-T.; Chang, C.-F.; Muralidhar Reddy, P.; Velmurugan, B.K. A Review on the Effects of Current Chemotherapy Drugs and Natural Agents in Treating Non-Small Cell Lung Cancer. *BioMedicine* **2017**, *7*, 23. [CrossRef] [PubMed]
13. Joulia, J.M.; Pinguet, F.; Grosse, P.Y.; Astre, C.; Bressolle, F. Determination of 5-Fluorouracil and Its Main Metabolites in Plasma by High-Performance Liquid Chromatography: Application to a Pharmacokinetic Study. *J. Chromatogr. B Biomed. Sci. Appl.* **1997**, *692*, 427–435. [CrossRef]
14. Escoriaza, J.; Aldaz, A.; Calvo, E.; Giráldez, J. Simple and Sensitive Determination of 5-Fluorouracil in Plasma by High-Performance Liquid Chromatography. *J. Chromatogr. B Biomed. Sci. Appl.* **1999**, *736*, 97–102. [CrossRef]
15. Langer, R. New Methods of Drug Delivery. *Science* **1990**, *249*, 1527–1533. [CrossRef]
16. Raza, A.; Hayat, U.; Rasheed, T.; Bilal, M.; Iqbal, H.M.N. "Smart" Materials-Based near-Infrared Light-Responsive Drug Delivery Systems for Cancer Treatment: A Review. *J. Mater. Res. Technol.* **2019**, *8*, 1497–1509. [CrossRef]
17. Pooresmaeil, M.; Namazi, H.; Salehi, R. Photoluminescent Folic Acid Functionalized Biocompatible and Stimuli-Responsive Nanostructured Polymer Brushes for Targeted and Controlled Delivery of Doxorubicin. *Eur. Polym. J.* **2021**, *156*, 110610. [CrossRef]
18. Pooresmaeil, M.; Nia, S.B.; Namazi, H. Green Encapsulation of LDH (Zn/Al)-5-Fu with Carboxymethyl Cellulose Biopolymer; New Nanovehicle for Oral Colorectal Cancer Treatment. *Int. J. Biol. Macromol.* **2019**, *139*, 994–1001. [CrossRef] [PubMed]
19. Yao, C.; Tian, J.; Wang, H.; Zhang, D.-W.; Liu, Y.; Zhang, F.; Li, Z.-T. Loading-Free Supramolecular Organic Framework Drug Delivery Systems (Sof-DDSs) for Doxorubicin: Normal Plasm and Multidrug Resistant Cancer Cell-Adaptive Delivery and Release. *Chin. Chem. Lett.* **2017**, *28*, 893–899. [CrossRef]
20. Mandal, A.S.; Biswas, N.; Karim, K.M.; Guha, A.; Chatterjee, S.; Behera, M.; Kuotsu, K. Drug Delivery System Based on Chronobiology—A Review. *J. Control. Release* **2010**, *147*, 314–325. [CrossRef] [PubMed]

21. Pooresmaeil, M.; Asl, E.A.; Namazi, H. A New PH-Sensitive CS/Zn-MOF@GO Ternary Hybrid Compound as a Biofriendly and Implantable Platform for Prolonged 5-Fluorouracil Delivery to Human Breast Cancer Cells. *J. Alloy. Compd.* **2021**, *885*, 160992. [CrossRef]
22. Farokhzad, O.C.; Langer, R. Impact of Nanotechnology on Drug Delivery. *ACS Nano* **2009**, *3*, 16–20. [CrossRef]
23. Tatlisoz, M.M.; Demirturk, E.; Canpolat, C. Release Characteristics of Gliclazide in a Matrix System. *Silico Pharmacol.* **2021**, *9*, 12. [CrossRef] [PubMed]
24. Wilczewska, A.Z.; Niemirowicz, K.; Markiewicz, K.H.; Car, H. Nanoparticles as Drug Delivery Systems. *Pharmacol. Rep.* **2012**, *64*, 1020–1037. [CrossRef]
25. Singh, R.; Lillard, J.W. Nanoparticle-Based Targeted Drug Delivery. *Exp. Mol. Pathol.* **2009**, *86*, 215–223. [CrossRef] [PubMed]
26. Tian, Y.; Tian, Z.; Dong, Y.; Wang, X.; Zhan, L. Current Advances in Nanomaterials Affecting Morphology, Structure, and Function of Erythrocytes. *RSC Adv.* **2021**, *11*, 6958–6971. [CrossRef]
27. Szefler, B. Nanotechnology, from Quantum Mechanical Calculations up to Drug Delivery. *Int. J. Nanomed.* **2018**, *13*, 6143–6176. [CrossRef]
28. Pooresmaeil, M.; Namazi, H. Preparation and Characterization of Polyvinyl Alcohol/β-Cyclodextrin/GO-Ag Nanocomposite with Improved Antibacterial and Strength Properties. *Polym. Adv. Technol.* **2019**, *30*, 447–456. [CrossRef]
29. Scicluna, M.C.; Vella-Zarb, L. Evolution of Nanocarrier Drug-Delivery Systems and Recent Advancements in Covalent Organic Framework–Drug Systems. *ACS Appl. Nano Mater.* **2020**, *3*, 3097–3115. [CrossRef]
30. Karimzadeh, Z.; Javanbakht, S.; Namazi, H. Carboxymethylcellulose/MOF-5/Graphene Oxide Bio-Nanocomposite as Antibacterial Drug Nanocarrier Agent. *BioImpacts* **2018**, *9*, 5–13. [CrossRef] [PubMed]
31. Yan, J.; Ye, Z.; Chen, M.; Liu, Z.; Xiao, Y.; Zhang, Y.; Zhou, Y.; Tan, W.; Lang, M. Fine Tuning Micellar Core-Forming Block of Poly(Ethylene Glycol)- Block -Poly(ε-Caprolactone) Amphiphilic Copolymers Based on Chemical Modification for the Solubilization and Delivery of Doxorubicin. *Biomacromolecules* **2011**, *12*, 2562–2572. [CrossRef]
32. Yang, Y.; Ostadhosseini, N. A Theoretical Investigation on the Mercaptopurine Drug Interaction with Boron Nitride Nanocage: Solvent and Density Functional Effect. *Phys. E Low-Dimens. Syst. Nanostructures* **2021**, *125*, 114337. [CrossRef]
33. Mohammed, M.H.; Hanoon, F.H. Theoretical Prediction of Delivery and Adsorption of Various Anticancer Drugs into Pristine and Metal-Doped Graphene Nanosheet. *Chin. J. Phys.* **2020**, *68*, 578–595. [CrossRef]
34. Ding, C.; Li, Z. A Review of Drug Release Mechanisms from Nanocarrier Systems. *Mater. Sci. Eng. C Mater. Biol. Appl.* **2017**, *76*, 1440–1453. [CrossRef] [PubMed]
35. Lee, J.H.; Yeo, Y. Controlled Drug Release from Pharmaceutical Nanocarriers. *Chem. Eng. Sci.* **2015**, *125*, 75–84. [CrossRef] [PubMed]
36. Kamaly, N.; Yameen, B.; Wu, J.; Farokhzad, O.C. Degradable Controlled-Release Polymers and Polymeric Nanoparticles: Mechanisms of Controlling Drug Release. *Chem. Rev.* **2016**, *116*, 2602–2663. [CrossRef]
37. Austin, L.A.; Mackey, M.A.; Dreaden, E.C.; El-Sayed, M.A. The Optical, Photothermal, and Facile Surface Chemical Properties of Gold and Silver Nanoparticles in Biodiagnostics, Therapy, and Drug Delivery. *Arch. Toxicol.* **2014**, *88*, 1391–1417. [CrossRef]
38. Kudr, J.; Haddad, Y.; Richtera, L.; Heger, Z.; Cernak, M.; Adam, V.; Zitka, O. Magnetic Nanoparticles: From Design and Synthesis to Real World Applications. *Nanomaterials* **2017**, *7*, 243. [CrossRef]
39. Malik, N.; Evagorou, E.G.; Duncan, R. Dendrimer-Platinate. *Anticancer Drugs* **1999**, *10*, 767–776. [CrossRef]
40. Nakanishi, T.; Fukushima, S.; Okamoto, K.; Suzuki, M.; Matsumura, Y.; Yokoyama, M.; Okano, T.; Sakurai, Y.; Kataoka, K. Development of the Polymer Micelle Carrier System for Doxorubicin. *J. Control. Release* **2001**, *74*, 295–302. [CrossRef]
41. Batrakova, E.V.; Dorodnych, T.Y.; Klinskii, E.Y.; Kliushnenkova, E.N.; Shemchukova, O.B.; Goncharova, O.N.; Arjakov, S.A.; Alakhov, V.Y.; Kabanov, A. V Anthracycline Antibiotics Non-Covalently Incorporated into the Block Copolymer Micelles: In Vivo Evaluation of Anti-Cancer Activity. *Br. J. Cancer* **1996**, *74*, 1545–1552. [CrossRef]
42. Rivera, E. Current Status of Liposomal Anthracycline Therapy in Metastatic Breast Cancer. *Clin. Breast Cancer* **2003**, *4* (Suppl. 2), S76–S83. [CrossRef] [PubMed]
43. Rosenthal, E.; Poizot-Martin, I.; Saint-Marc, T.; Spano, J.-P.; Cacoub, P. Phase IV Study of Liposomal Daunorubicin (DaunoXome) in AIDS-Related Kaposi Sarcoma. *Am. J. Clin. Oncol.* **2002**, *25*, 57–59. [CrossRef] [PubMed]
44. Volkov, Y. Quantum Dots in Nanomedicine: Recent Trends, Advances and Unresolved Issues. *Biochem. Biophys. Res. Commun.* **2015**, *468*, 419–427. [CrossRef] [PubMed]
45. Pastorin, G.; Wu, W.; Wieckowski, S.; Briand, J.-P.; Kostarelos, K.; Prato, M.; Bianco, A. Double Functionalisation of Carbon Nanotubes for Multimodal Drug Delivery. *Chem. Commun.* **2006**, 1182–1184. [CrossRef] [PubMed]
46. Wu, W.; Wieckowski, S.; Pastorin, G.; Benincasa, M.; Klumpp, C.; Briand, J.-P.; Gennaro, R.; Prato, M.; Bianco, A. Targeted Delivery of Amphotericin B to Cells by Using Functionalized Carbon Nanotubes. *Angew. Chem. Int. Ed. Engl.* **2005**, *44*, 6358–6362. [CrossRef] [PubMed]
47. Chimene, D.; Alge, D.L.; Gaharwar, A.K. Two-Dimensional Nanomaterials for Biomedical Applications: Emerging Trends and Future Prospects. *Adv. Mater.* **2015**, *27*, 7261–7284. [CrossRef]
48. Tan, C.; Cao, X.; Wu, X.-J.; He, Q.; Yang, J.; Zhang, X.; Chen, J.; Zhao, W.; Han, S.; Nam, G.-H.; et al. Recent Advances in Ultrathin Two-Dimensional Nanomaterials. *Chem. Rev.* **2017**, *117*, 6225–6331. [CrossRef]
49. Luan, B.; Zhou, R. Spontaneous Transport of Single-Stranded DNA through Graphene–MoS 2 Heterostructure Nanopores. *ACS Nano* **2018**, *12*, 3886–3891. [CrossRef]

50. Duan, F.; Zhang, S.; Yang, L.; Zhang, Z.; He, L.; Wang, M. Bifunctional Aptasensor Based on Novel Two-Dimensional Nanocomposite of MoS2 Quantum Dots and g-C3N4 Nanosheets Decorated with Chitosan-Stabilized Au Nanoparticles for Selectively Detecting Prostate Specific Antigen. *Anal. Chim. Acta* **2018**, *1036*, 121–132. [CrossRef]
51. Peng, L.; Mei, X.; He, J.; Xu, J.; Zhang, W.; Liang, R.; Wei, M.; Evans, D.G.; Duan, X. Monolayer Nanosheets with an Extremely High Drug Loading toward Controlled Delivery and Cancer Theranostics. *Adv. Mater.* **2018**, *30*, 1707389. [CrossRef]
52. Xie, Z.; Wang, D.; Fan, T.; Xing, C.; Li, Z.; Tao, W.; Liu, L.; Bao, S.; Fan, D.; Zhang, H. Black Phosphorus Analogue Tin Sulfide Nanosheets: Synthesis and Application as near-Infrared Photothermal Agents and Drug Delivery Platforms for Cancer Therapy. *J. Mater. Chem. B* **2018**, *6*, 4747–4755. [CrossRef] [PubMed]
53. Chen, W.; Ouyang, J.; Liu, H.; Chen, M.; Zeng, K.; Sheng, J.; Liu, Z.; Han, Y.; Wang, L.; Li, J. Black Phosphorus Nanosheet-based Drug Delivery System for Synergistic Photodynamic/Photothermal/Chemotherapy of Cancer. *Adv. Mater.* **2017**, *29*, 1603864. [CrossRef]
54. Javanbakht, S.; Nazari, N.; Rakhshaei, R.; Namazi, H. Cu-Crosslinked Carboxymethylcellulose/Naproxen/Graphene Quantum Dot Nanocomposite Hydrogel Beads for Naproxen Oral Delivery. *Carbohydr. Polym.* **2018**, *195*, 453–459. [CrossRef] [PubMed]
55. Murray, C.B.; Norris, D.J.; Bawendi, M.G. Synthesis and Characterization of Nearly Monodisperse CdE (E = Sulfur, Selenium, Tellurium) Semiconductor Nanocrystallites. *J. Am. Chem. Soc.* **1993**, *115*, 8706–8715. [CrossRef]
56. Pagliai, M.; Caporali, S.; Muniz-Miranda, M.; Pratesi, G.; Schettino, V. SERS, XPS, and DFT Study of Adenine Adsorption on Silver and Gold Surfaces. *J. Phys. Chem. Lett.* **2012**, *3*, 242–245. [CrossRef]
57. Chai, J.-D.; Head-Gordon, M. Long-Range Corrected Hybrid Density Functionals with Damped Atom–Atom Dispersion Corrections. *Phys. Chem. Chem. Phys.* **2008**, *10*, 6615. [CrossRef] [PubMed]
58. Yar, M.; Ayub, K. Expanding the Horizons of Covalent Organic Frameworks to Electrochemical Sensors; A Case Study of CTF-FUM. *Microporous Mesoporous Mater.* **2020**, *300*, 110146. [CrossRef]
59. Ahmad Farooqi, B.; Yar, M.; Ashraf, A.; Farooq, U.; Ayub, K. Graphene-Polyaniline Composite as Superior Electrochemical Sensor for Detection of Cyano Explosives. *Eur. Polym. J.* **2020**, *138*, 109981. [CrossRef]
60. Yar, M.; Hashmi, M.A.; Ayub, K. Nitrogenated Holey Graphene (C2N) Surface as Highly Selective Electrochemical Sensor for Ammonia. *J. Mol. Liq.* **2019**, *296*, 111929. [CrossRef]
61. Yar, M.; Hashmi, M.A.; Ayub, K. The C2N Surface as a Highly Selective Sensor for the Detection of Nitrogen Iodide from a Mixture of NX3 (X = Cl, Br, I) Explosives. *RSC Adv.* **2020**, *10*, 31997–32010. [CrossRef] [PubMed]
62. Pan, S.; Saha, R.; Mandal, S.; Mondal, S.; Gupta, A.; Fernández-Herrera, M.A.; Merino, G.; Chattaraj, P.K. Selectivity in Gas Adsorption by Molecular Cucurbit[6]Uril. *J. Phys. Chem. C* **2016**, *120*, 13911–13921. [CrossRef]
63. Keinan, S.; Contreras-García, J.; Johnson, E.R.; Yang, W.; Mori-Sánchez, P.; Cohen, A.J. Revealing Noncovalent Interactions. *J. Am. Chem. Soc.* **2010**, *132*, 6498–6506. [CrossRef]
64. Contreras-García, J.; Johnson, E.R.; Keinan, S.; Chaudret, R.; Piquemal, J.-P.; Beratan, D.N.; Yang, W. NCIPLOT: A Program for Plotting Noncovalent Interaction Regions. *J. Chem. Theory Comput.* **2011**, *7*, 625–632. [CrossRef]
65. Contreras-García, J.; Yang, W.; Johnson, E.R. Analysis of Hydrogen-Bond Interaction Potentials from the Electron Density: Integration of Noncovalent Interaction Regions. *J. Phys. Chem. A* **2011**, *115*, 12983–12990. [CrossRef]
66. Venkataramanan, N.S.; Suvitha, A.; Kawazoe, Y. Unravelling the Nature of Binding of Cubane and Substituted Cubanes within Cucurbiturils: A DFT and NCI Study. *J. Mol. Liq.* **2018**, *260*, 18–29. [CrossRef]
67. Doust Mohammadi, M.; Abdullah, H.Y. The Adsorption of Chlorofluoromethane on Pristine, Al-, Ga-, P-, and As-Doped Boron Nitride Nanotubes: A PBC-DFT, NBO, and QTAIM Study. *ChemistrySelect* **2020**, *5*, 12115–12124. [CrossRef]
68. Chu, Z.Q.; Stampfl, C.; Duan, X.M. Boron-Doped g-C6N6 Layer as a Metal-Free Photoelectrocatalyst for N2 Reduction Reaction. *J. Phys. Chem. C* **2019**, *123*, 28739–28743. [CrossRef]
69. Munir, M.; Ahsan, F.; Yar, M.; Ayub, K. Theoretical Investigation of Double-Cubed Polycationic Cluster (Sb7Se8Cl2)3+ for the Storage of Helium and Neon. *Mater. Sci. Semicond. Process.* **2022**, *148*, 106756. [CrossRef]
70. Srinivasu, K.; Modak, B.; Ghosh, S.K. Porous Graphitic Carbon Nitride: A Possible Metal-Free Photocatalyst for Water Splitting. *J. Phys. Chem. C* **2014**, *118*, 26479–26484. [CrossRef]
71. Li, T.; Zhang, W.-D.; Liu, Y.; Li, Y.; Cheng, C.; Zhu, H.; Yan, X.; Li, Z.; Gu, Z.-G. A Two-Dimensional Semiconducting Covalent Organic Framework with Nickel(ii) Coordination for High Capacitive Performance. *J. Mater. Chem. A* **2019**, *7*, 19676–19681. [CrossRef]
72. Longley, D.B.; Harkin, D.P.; Johnston, P.G. 5-Fluorouracil: Mechanisms of Action and Clinical Strategies. *Nat. Rev. Cancer* **2003**, *3*, 330–338. [CrossRef] [PubMed]
73. Schallreuter, K.U.; Gleason, F.K.; Wood, J.M. The Mechanism of Action of the Nitrosourea Anti-Tumor Drugs on Thioredoxin Reductase, Glutathione Reductase and Ribonucleotide Reductase. *Biochim. Biophys. Acta-Mol. Cell Res.* **1990**, *1054*, 14–20. [CrossRef]
74. Kumar, P.S.V.; Raghavendra, V.; Subramanian, V. Bader's Theory of Atoms in Molecules (AIM) and Its Applications. *J. Chem. Sci.* **2016**, *128*, 1527–1536. [CrossRef]
75. Espinosa, E.; Molins, E.; Lecomte, C. Hydrogen Bond Strengths Revealed by Topological Analyses of Experimentally Observed Electron Densities. *Chem. Phys. Lett.* **1998**, *285*, 170–173. [CrossRef]
76. Parthasarathi, R.; Subramanian, V.; Sathyamurthy, N. Hydrogen Bonding without Borders: An Atoms-in-Molecules Perspective. *J. Phys. Chem. A* **2006**, *110*, 3349–3351. [CrossRef]

77. Espinosa, E.; Alkorta, I.; Elguero, J.; Molins, E. From Weak to Strong Interactions: A Comprehensive Analysis of the Topological and Energetic Properties of the Electron Density Distribution Involving X–H···F–Y Systems. *J. Chem. Phys.* **2002**, *117*, 5529–5542. [CrossRef]
78. Xie, C.; Li, P.; Han, L.; Wang, Z.; Zhou, T.; Deng, W.; Wang, K.; Lu, X. Electroresponsive and Cell-Affinitive Polydopamine/Polypyrrole Composite Microcapsules with a Dual-Function of on-Demand Drug Delivery and Cell Stimulation for Electrical Therapy. *NPG Asia Mater.* **2017**, *9*, e358. [CrossRef]
79. Chapman, C.A.R.; Cuttaz, E.A.; Goding, J.A.; Green, R.A. Actively Controlled Local Drug Delivery Using Conductive Polymer-Based Devices. *Appl. Phys. Lett.* **2020**, *116*, 010501. [CrossRef]
80. Ahsan, F.; Yar, M.; Gulzar, A.; Ayub, K. Therapeutic Potential of C2N as Targeted Drug Delivery System for Fluorouracil and Nitrosourea to Treat Cancer: A Theoretical Study. *J. Nanostructure Chem.* **2022**. [CrossRef]
81. Shakerzadeh, E. Efficient Carriers for Anticancer 5-Fluorouracil Drug Based on the Bare and M−encapsulated (M = Na and Ca) B40 Fullerenes; in Silico Investigation. *J. Mol. Liq.* **2021**, *343*, 116970. [CrossRef]
82. Tabtimsai, C.; Wanno, B. Theoretical Investigation on 5–Fluorouracil Anti–Cancer Drug Adsorption on Sc– and Ti–Doped Armchair and Zigzag Boron Nitride Nanotubes. *J. Mol. Liq.* **2021**, *337*, 116596. [CrossRef]
83. Rahimi, R.; Solimannejad, M. BC3 Graphene-like Monolayer as a Drug Delivery System for Nitrosourea Anticancer Drug: A First-Principles Perception. *Appl. Surf. Sci.* **2020**, *525*, 146577. [CrossRef]
84. Shakerzadeh, E.; Tahmasebi, E.; Van Duong, L.; Tho Nguyen, M. Boron Clusters in Biomedical Applications: A Theoretical Viewpoint. In *Characteristics and Applications of Boron*; IntechOpen: London, UK, 2022.